Self-recognition of the racemic ligand in the formation of homochiral dinuclear V(V) complex: In vitro anticancer activity, DNA and HSA interaction

Zahra Kazemi, Hadi Amiri Rudbari, Valiollah Mirkhani, Mehdi Sahihi, Majid Moghadam, Shahram Tangestaninejad, Iraj Mohammadpoor-Baltork, Abolghasem Abbasi Kajani, Gholamhassan Azimi

Self-recognition of the racemic ligand in the formation of homochiral dinuclear V(V) complex: In vitro anticancer activity, DNA and HSA interaction

Zahra Kazemi, Hadi Amiri
Rudbari, Valiollah Mirkhani, Mehdi Sahihi, Majid Moghadam, Shahram Tangestaninejad, Iraj M ohammadpoor-Baltork, Abolghasem Abbasi Kajani, Gholamhassan Azimi

Department of Chemistry, University of Isfahan, Isfahan, 81746-73441, Iran

Abstract

The reaction of a racemic mixture of Schiff base tridentate ligand with vanadium(V) affords homochiral vanadium complex, $(VO(R\text{-}L))_2O$ and $(VO(S\text{-}L))_2O$ due to ligand "self-recognition" process. The formation of homochiral vanadium complex was confirmed by ^{1}H NMR, ^{13}C NMR and X-ray diffraction. The HSA- and DNA-binding of the resultant complex is assessed by absorption, fluorescence and circular dichroism (CD) spectroscopy methods. Based on the results, the HSA- and DNA-binding constant, K_b, were found to be 8.0×10^4 and 1.9×10^5 M^{-1}, respectively. Interestingly, in vitro cytotoxicity assay revealed the potent anticancer activity of this complex on two prevalent cancer cell lines of MCF-7 (IC50 value of 14 μM) and HeLa (IC50 value of 36 μM), with considerably low toxicity on normal human fibroblast cells. The maximum cell mortality of 12.3% obtained after 48 h incubation of fibroblast cells with 100 μM of the complex. Additionally, the specific DNA- and HSA-binding was also shown using molecular docking method. The synthesized complex displayed high potential for biomedical applications especially for development of novel and efficient anticancer agents.

Keywords

Dinuclear vanadium complex

Self-recognition

Homochiral metal complex

DNA- and HSA-binding

In vitro assay

1. Introduction

Chirality is the main feature of living world. It is an important phenomenon not only in the human life but also in food flavors, medicinal, pharmaceutical, agricultural, catalysis and other chemical industries [1], [2], [3]. In this field, process of molecular self-recognition plays a vital role, by which the stereoselective synthesis of coordination compounds can be feasible [4]. In this process, each enantiomeric ligand selectively recognizes itself to produce a homochiral complex [4]. One example of using chiral ligand to induce self-recognition is dinuclear complexes. In these cases, the self-recognition process affords homochiral complex ($[M_2(R\text{-}L)_2]^{n+}$ or $[M_2(S\text{-}L)_2]^{n+}$ species) in excess of heterochiral one ($[M_2(R,S\text{-}L)]^{n+}$), even when a racemic mixture of ligand (L) is used [5].

The researches have been shown that multi nuclear metal complexes possess different spectrum of anti-cancer activity [6], and they are also among the best studied of nonclassical anticancer agents [7]. Binuclear platinum complexes have attracted much attention because of their higher activity in vitro and *in vivo* than their monomeric analogues [8].
Among the transition metal ions used in pharmacological studies, vanadium is one of the most promising anticancer drug. Vanadium compounds possess some medicinal uses including antiviral, antiparasitic, antibacterial and also therapeutic potential in diabetes [9], [10], [11]. The origin of anticancer activity of vanadium compounds is disruption of cellular metabolism through the generation of ROS and also their ability on DNA damage [9], [12]. Its compounds can be as possible alternatives to platinum-based metal complexes [13].
Previously, we have used a racemic ligand to synthesis racemic and *meso* forms of Pd(II) complexes and their biological activities were studied [14]. In the present study, in continuation of previous work a racemic mixture of Schiff base ligand was used to synthesis vanadium complex. It is interesting to note that although a racemic mixture of ligand is employed, the resultant dimeric complex comprises homochiral dimers solely. There are possibility to form four isomers upon complexation, but the isolated complex was a racemic mixture of the homochiral isomer, $(VO(S,S\text{-}L))_2O$ and $(VO(R,R\text{-}L))_2O$, due to ligand self-recognition (Scheme 1). In the process of complexation, the chiral recognition is occurred, similar to previous studies [4], [5]. X-ray diffraction and NMR techniques have been used to confirm this synthesis. DNA- and HSA-binding of the homochiral complex have been evaluated by means of both experimental (fluorescence quenching, UV–Vis spectroscopy and circular dichroism (CD) methods) and computational methods (molecular docking). During this study, its in vitro cytotoxic activity against human cell lines (MCF-7 and HeLa) and normal human fibroblast cells was also carried out.

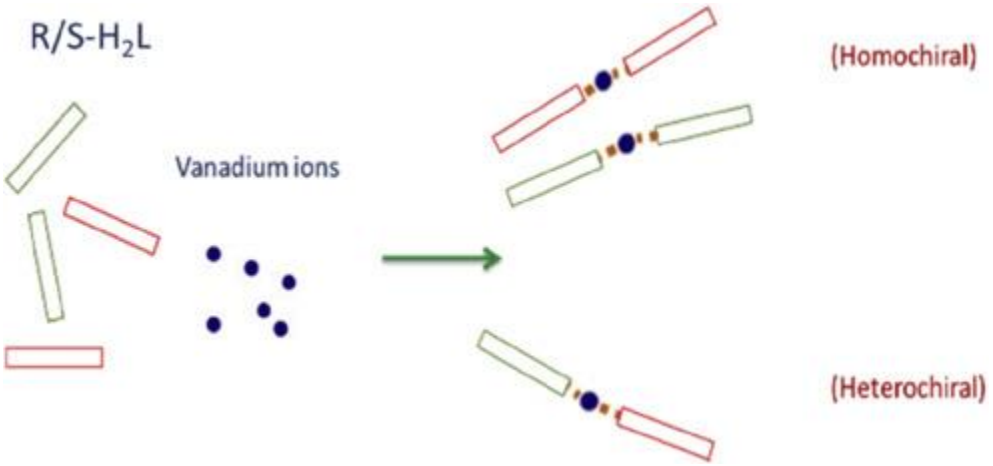

Scheme 1. The scheme of synthesis homo and heterochiral dinuclear vanadium complex.

2. Result and discussion

2.1. Synthesis and characterization

The pKa of a drug can influence on many parameters including lipophilicity, solubility, protein binding, and permeability which in turn directly affects pharmacokinetic characteristics such as absorption, distribution, metabolism, and excretion [15], [16]. Study of pKa value can give

information about the ionic form of a drug and also the rate at which it is able to diffuse across membranes and obstacles [16]. There are some literature that determined pKa of compounds along with their biological activities [17], [18].

Therefore, in this work the pKa values of hydroxyl groups of the Schiff base ligand has been calculated by Marvin V.5.1 software (https://www.chemaxon.com/products/marvin/). This ligand has two pKa values because of existence two different hydroxyl groups which are obtained as 8.13 and 15.56 for phenolic and aliphatic hydroxyl groups, respectively. The first (pKa_1) and second dissociation equilibriums (pKa_2) of the ligand refer to the phenolic and aliphatic OH, respectively. In addition, from the reaction of the Schiff base ligand with $V(IV)O(acac)_2$ dinuclear V(V) complex has been formed. In this reaction V(IV) was oxidized by O_2 of air and the oxidation state of the vanadium atom has been changed from IV to V. This change in vanadium oxidation state can be easily occur in some reactions [19], [20]. The synthetic pathway for the novel dinuclear V(V) complex from a racemic Schiff base ligand is depicted in Scheme 2. Here, although a racemic ligand was employed, the complex is isolated as a homochiral isomer. This observation can be explained by self-recognition process of ligand.

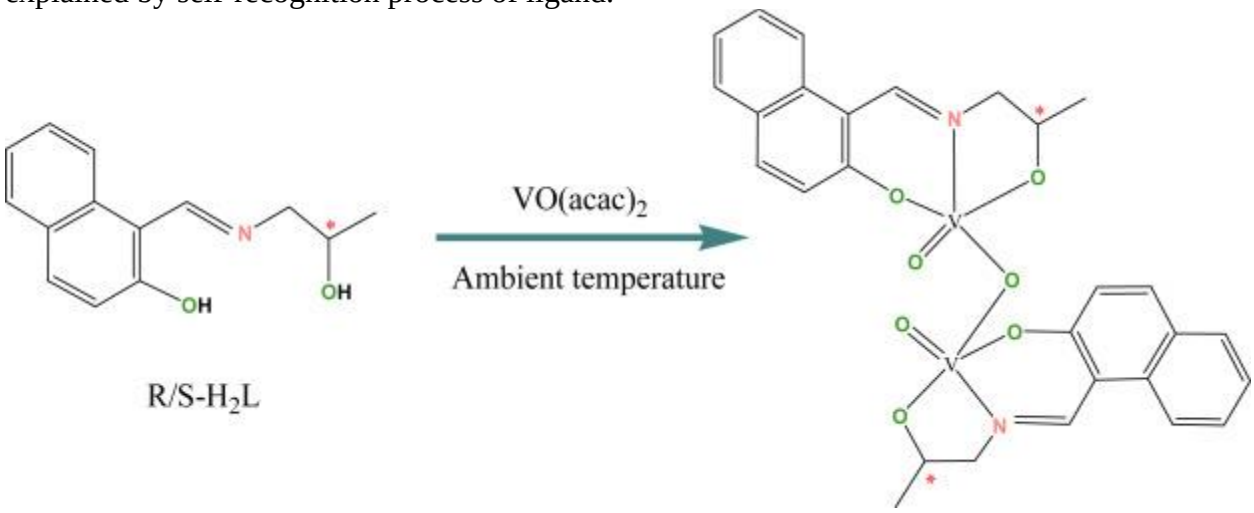

Scheme 2. Synthesis of V(V) complex.

The V(V) complex was characterized by ^1H NMR, ^{13}C NMR, FT-IR, elemental analysis techniques and X-ray diffraction. Characteristic IR bands and their assignments are given in the experimental section. In the FT-IR spectra of the complex the absence of the phenolic O—H vibration is indicative of deprotonation of ligand to coordination through oxygen atom. The stretching band of the imine group (C=N) appeared at 1621 cm^{-1} [21]. The strong bands related to the C—O and C—N stretching were observed at the region of 1339 and 1541 cm^{-1}. In addition, absorption bands around 987 and 748 cm^{-1} can be attributed to V=O and V–O–V moieties, respectively [22].

The proton NMR spectrum of the complex was collected in $CDCl_3$ (Fig. S1). This technique is the easiest way to measure the homochiral purity of the complex. The appearance of single peak for protons demonstrated 100% of the resultant precipitate is homochiral and no trace of the heterochiral species was found. A characteristics feature of the ^1H NMR spectrum of the complex is the imine proton resonance (H_1), observing at 8.6 ppm. The resonance signal corresponding to phenolic (OH) proton disappears in the V(V) complex, indicating the coordination of oxygen atom to V(V) ion. The protons H_{2a} and H_{2b} are diastereotopic ones, therefore they split each other and have different chemical shifts. The related signals are appeared as doublet of doublet, at 3.4 and

3.7 ppm. The signal (m, 1H) at 4.1 ppm is due to –CH (H_3). The doublet signal at 1.3 ppm is attributed to the CH_3. The aromatic protons are observed in the ranged 6.7–7.7 ppm. The ^{13}C NMR spectra of V(V) complex show 14 signals (Fig. S2). The peak observed at 177.7 ppm is ascribed to the imine carbon atom. The existence this peak in the spectrum of complex supports the presence of the Schiff base in the complex. The peaks in the range of 106.2–159.0 ppm is assigned to aromatic protons.

The formation of homochiral V(V) complex was also confirmed by single crystal X-ray diffraction analysis. The crystallographic data and the selected bond lengths and angles are collected in Table 1, Table 2, respectively. The complex crystallizes in space group C2/c and a representative ORTEP view of one of enantiomeric pairs, $(VO(R,R\text{-L}))_2O$, is presented in Fig. 1. The complex contains a stereogenic center at atom C13 (Fig. 1) and the reference molecule was selected as one having the *R*-configuration at atom C13. The centrosymmetric space group confirms the crystals comprise a racemic mixture of $(VO(S,S\text{-L}))_2O$ and $(VO(R,R\text{-L}))_2O$ (Fig. 2).

Table 1. Crystal data and structure refinement for **$(VOL)_2O$**.

Empirical formula	$C_{32}H_{34}N_2O_8V_2$
Formula weight	676.49
Temperature (K)	298(2)
Wavelength (Å)	0.71073 Å
Crystal system	Monoclinic
Space group	C 2/c
Unit cell dimensions (Å, °)	a = 17.053(3) Å
	b = 11.257(2) Å
	c = 18.914(4) Å
	β = 103.64(3)°
Volume ($Å^3$)	3528.6(13) $Å^3$
Z	4
Calculated density (Mg/m^3)	1.273 Mg/m^3
Absorption coefficient (mm^{-1})	0.541 mm^{-1}
F(000)	1400
Theta range for data collection (°)	2.896 to 29.281
Index ranges	$-23 \leq h = 22$
	$-15 \leq k = 15$
	$0 \leq l = 25$
Reflections collected	9219

Independent reflections	4758 [$R_{(int)}$ = 0.0607]
Data Completeness (%)	99.8
Refinement method	Full-matrix least-squares on F^2
Data/restraints/parameters	4758/0/223
Goodness-of-fit on F^2	0.965
Final R indices [I > 2σ (I)]	R_1 = 0.0947
	wR_2 = 0.2579
R indices (all data)	R_1 = 0.1711
	wR_2 = 0.2790
Largest diff. peak and hole (e.Å^{-3})	0.706 and −0.489 e.Å^{-3}

Table 2. Selected bond distances (Å) and angles (°) for (**VOL)$_2$O**.[a]

V(1)-O(1)	1.877(5)	O(3)-V(1)-O(4)	106.0(2)
V(1)-O(2)	1.905(3)	O(3)-V(1)-O(1)	102.1 (3)
V(1)-O(3)	1.592(5)	O(4)-V(1)-O(1)	99.3(17)
V(1)-O(4)	1.817(4)	O(3)-V(1)-O(2)	103.0(3)
V(1)-N(1)	2.080(6)	O(4)-V(1)-O(2)	88.0(19)
O(1)-C(1)	1.325(7)	O(1)-V(1)-O(2)	150.8(2)
O(2)-C(13)	1.415(8)	O(1)-V(1)-N(1)	82.3(2)
N(1)-C(11)	1.285(8)	O(2)-V(1)-N(1)	77.6(2)
N(1)-C(12)	1.470(8)	O(3)-V(1)-N(1)	103.0(3)
		O(4)-V(1)-N(1)	149.8(2)
		V(1)-O(4)-V(2)	107.1(3)

a Symmetry transformations used to generate equivalent atoms: 1 −x, −y, −z.

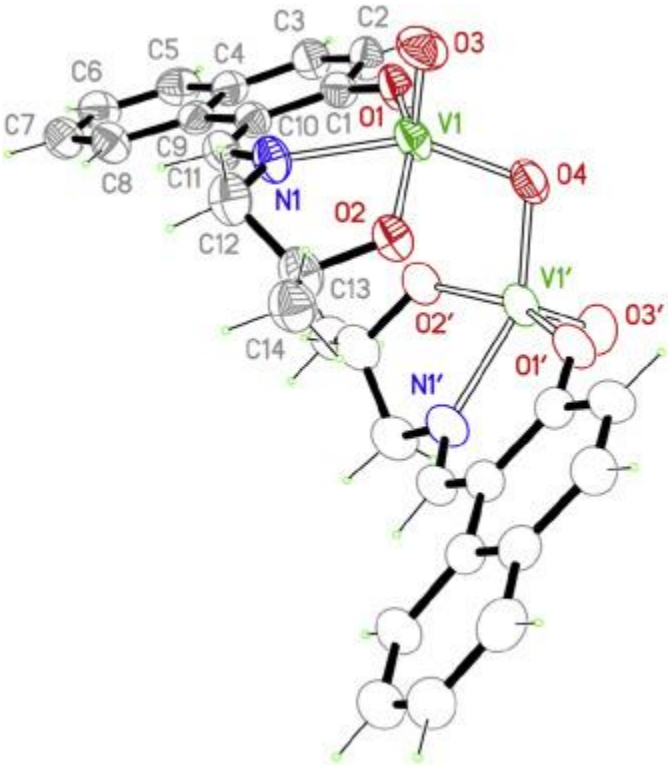

Fig. 1. View of $(VO(R,R\text{-}L))_2O$ evidencing the 2-fold axes passing through the oxygen atom (O4) and showing the numbering scheme of the asymmetric unit denoted by filled drawings. Displacement ellipsoids are drawn at the 30% probability level and H atoms are shown as small spheres of arbitrary radii.

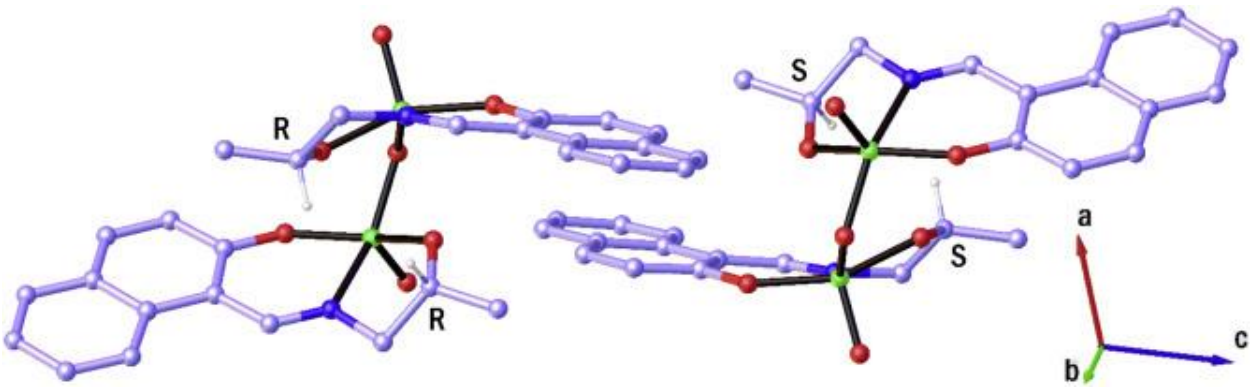

Fig. 2. Centrosymmetric space group confirms that the complex has crystallized as a racemic mixture.

The complex is a dinuclear species containing two V-centers with a tetrahydrofuran (THF) molecule as solvent. The vanadium center is surrounded by one oxo group, imine-N and two oxygen of a tridentate Schiff base ligand and an oxygen that acts as bridging group between two vanadium ions, therefore the coordination number of vanadium is five. To quantify the extent of distortion from either ideal square pyramid or trigonal bipyramid, the index of trigonality, τ, have been found from $\tau = (\alpha - \beta)/60$, α and β are the two largest bond angles around the metal atom in the five coordinated environment. For a perfectly square pyramidal (SP) geometry, τ should be

equal to zero, while it becomes unity for ideal trigonal bipyramidal (TBP) geometry. The τ value is 0.016 for **(VOL)$_2$O** and therefore the metal coordination geometry is described as almost ideal square pyramid with oxo-oxygen atom occupies the apical position.
The bond lengths and angles of the V(V) complex are comparable with their counterparts in the dinuclear vanadium complexes. The V…V bond lengths (2.923 Å) and the V–O–V bridge angle (107.1) are also in the expected range of dinuclear vanadium complexes [22], [23], [24], [25], [26].

2.2. DNA binding studies

2.2.1. Absorption spectroscopic studies

To gain insight into the nature of interaction between V(V) complex and DNA, electronic absorption of the complex in the absence or the presence of DNA were measured (Fig. 3). As shown in this figure, with the addition of FS-DNA a hyperchromism in absorption of V(V) complex was observed, indicating the complex can interact through groove binding mode [27].

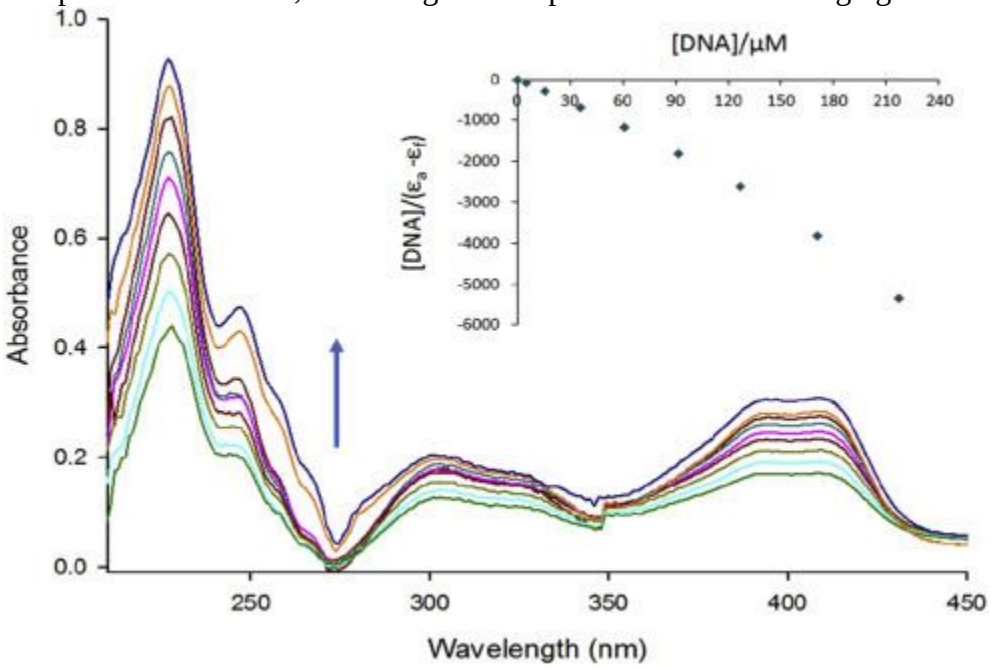

Fig. 3. The change of electronic absorption spectra of (**VOL)$_2$O** complex (2×10^{-5} M) upon addition various amounts of FS-DNA (2×10^{-4} M).

To quantitatively evaluate the affinity of compounds with FS-DNA, the intrinsic binding constant K_b was determined by monitoring the changes in absorbance using the following equation:

$$\frac{[DNA]}{\varepsilon_a - \varepsilon_f} = \frac{[DNA]}{\varepsilon_b - \varepsilon_f} + \frac{1}{K_b(\varepsilon_b - \varepsilon_f)} \quad (1)$$

where [DNA] is the concentration of FS-DNA; ε_a, ε_f and ε_b are the apparent extinction coefficient, the extinction coefficient for free compounds and the extinction coefficient for the compounds in fully bound form, respectively. ε_f was determined by calibration curve and ε_a is the ratio of A_{obs} to

[compound]. The K_b value was determined as ratio of slope to y-intercept of plot of [DNA]/(ε_a -ε_f) versus [DNA] and found as 1.4×10^5 M^{-1}.

2.2.2. Fluorescence study

The EthBr fluorescence displacement experiment was also employed to further investigate DNA-binding of V(V) complex, as previously reported [28]. Here, with the addition of the complex the fluorescence intensity of EthBr-DNA decreases continuously without any change in the emission λ_{max} (Fig. 4), suggesting possible binding of the complex to DNA. In order to determine the binding ability between the complex and FS-DNA, the Stern-Volmer quenching plot was obtained by monitoring the fluorescence quenching of the EthBr-DNA upon addition of the complex, according to the following equation [29]:

$$\frac{F_0}{F} = 1 + K_{sv}[Q] = 1 + k_q \tau [Q] \quad (2)$$

where, F_0 and F are the fluorescence intensity of EthBr-DNA complex in absence and presence of the complexes, respectively. [Q] is the concentration of quencher and K_{sv} is the Stern-Volmer quenching constant, k_q is the quenching rate constant of EthBr-DNA and τ is the average lifetime of EthBr-DNA without quencher which is typically equal to 10^{-8} s for biomacromolecules. K_{sv} is determined from the plot of F_0/F vs. [Q] (Fig. 4).

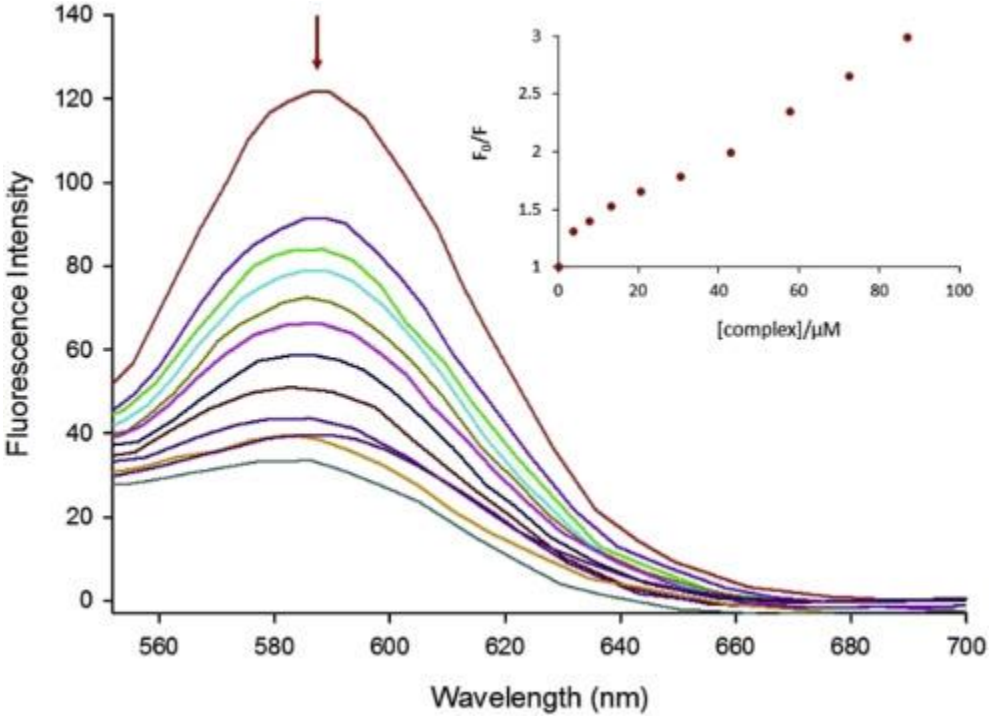

Fig. 4. Fluorescence spectra for titration of DNA: EthBr (50: 5 μM) with increasing amounts of **(VOL)$_2$O** (2.5×10^{-4} M), λ_{ex} = 520 nm.

Moreover, binding constant (K_b) of the complex and FS-DNA can be calculated by this experiment using equation (3) [30]:

$$\ln\left(\frac{F_0-F}{F}\right) = \ln K_b + n\ln[Q] \quad (3)$$

"K_b" is obtained from the plot of ln ((F$_0$-F)/F) versus ln [Q] as a y-intercept (Fig. S3). Furthermore, "n" which is the number of binding site per nucleic acid is slope of the plot. The values of K_{SV}, k_q and K_b were obtained as 2.2×10^4 M^{-1}, 2.2×10^{12} $M^{-1}S^{-1}$ and 1.9×10^5 M^{-1}, respectively.

2.2.3. Molecular docking of the V(V) complex with DNA

The molecular docking study was performed to predict the affinity and the binding orientation of the complex to DNA and HSA. The results revealed that the complex binds in the minor groove of DNA with the binding free energy (ΔG) of −8.28 kcal mol^{-1} (Fig. 5). This observation is completely consistent with the result of UV–Vis measurement. As shown in Fig. 6, the complex interacts with DG4, DG22, DA5 and DC21 nucleotides and formed three hydrogen bonds with them.

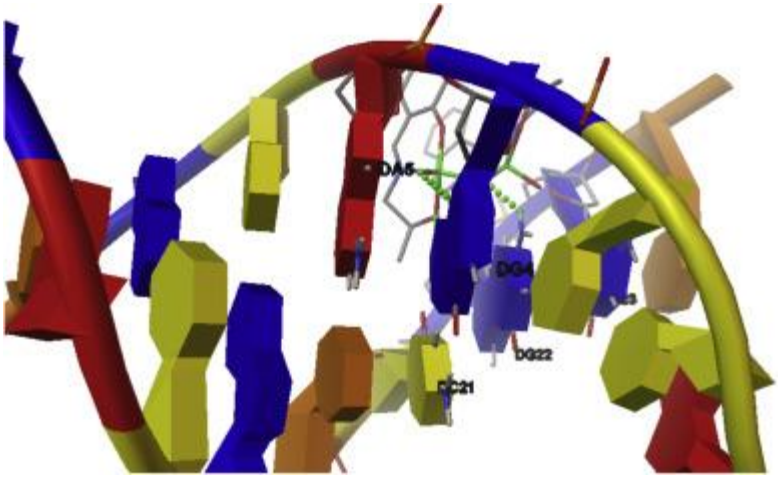

Fig. 5. Molecular docking poses for the interaction of $(VOL)_2O$ complex with DNA.

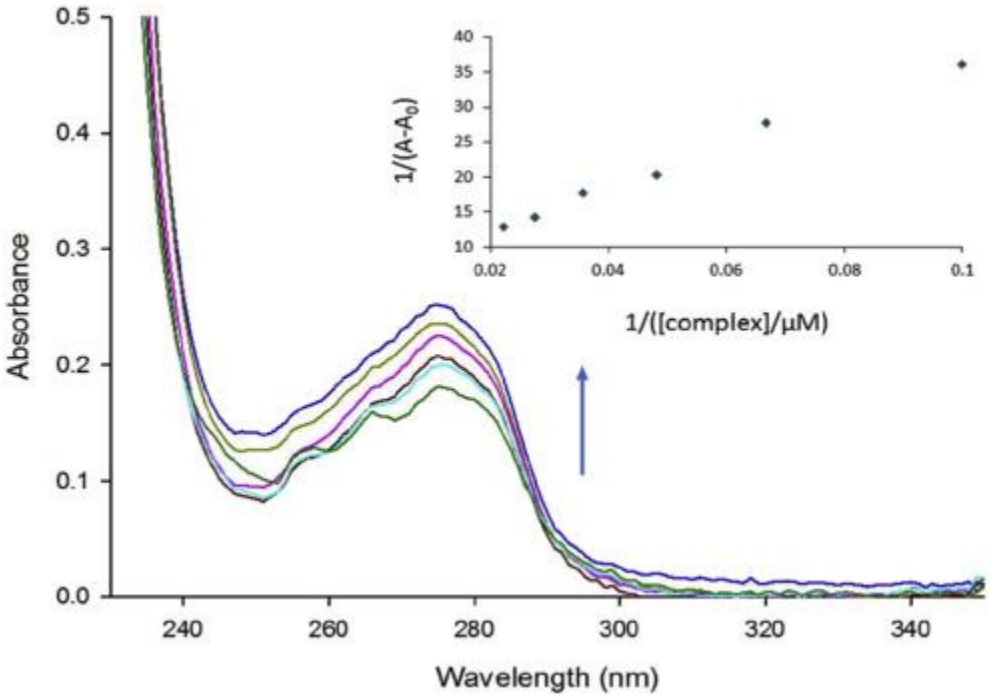

Fig. 6. The change of electronic absorption spectra of HSA (7×10^{-6} M) upon addition of various amounts of **(VOL)$_2$O** complex (7×10^{-5} M).

2.3. HSA binding studies

Protein binding of a drug increases drug solubility in plasma, decreases its toxicity, protects from oxidation, prevents rapid elimination of drugs from bloodstream and also prolongs its *in vivo* half-life [31], [32]. Hence, study of HSA-binding, the most abundant plasma protein, is required to design and synthesis a new drug.

2.3.1. Absorption spectroscopic studies

UV–Vis absorption spectroscopy carried out to study the HSA-drug binding and to investigate structural changes of protein upon its drug binding [33]. Through addition of V(V) complex, progressive increases was observed in the absorption peak of HSA at 278 nm (Fig. 6). This alteration in UV–Vis spectra can be related to interaction of the complex with HSA [34]. In order to assess the binding ability of the complex with HSA, the intrinsic binding constant (K_b) was determined by monitoring the changes of absorbance with increasing concentration of the complex and using Benesi–Hildebrand plot and equation (4) [35]:

$$\frac{1}{(A-A_0)} = \frac{1}{(A_{max}-A)} + \frac{1}{K_b(A_{max}-A)} \times \frac{1}{[M]} \quad (4)$$

where A_0 and A are the absorbance of HSA in the absence and presence of the complex, respectively. A_{max} is the obtained absorbance at saturation and [M] is the concentration of the complex. The plot of 1/(A−$\diamondsuit$0) versus1/[M] gives K_b as ratio of y-intercept to slop (Fig. 6) which in this study it is equal to 2.0×10^4 M^{-1}.

2.3.2. Fluorescence study

The addition of metal complexes to HSA can lead to decrease the fluorescence intensity of HSA, indicating the complexes interact with HSA and cause changes of microenvironment around the Trp-214 residue in HSA [36], [37]. In this work, the fluorescence quenching of HSA was measured at the presence of various amounts of the V(V) complex (Fig. 7). The values of K_{SV}, k_q and K_b were obtained as $2.1 \times 10^4\ M^{-1}$, $2.1 \times 10^{12}\ M^{-1}S^{-1}$ and $8.0 \times 10^4\ M^{-1}$, respectively (Eqs. (2), (3))) (Fig. S4). Furthermore, "*n*" which is the number of binding site per protein is nearly 1, indicating that the complex binds to HSA with molar ratio of 1:1 [36], [38]. The result is in good agreement with the UV–Vis spectroscopy result.

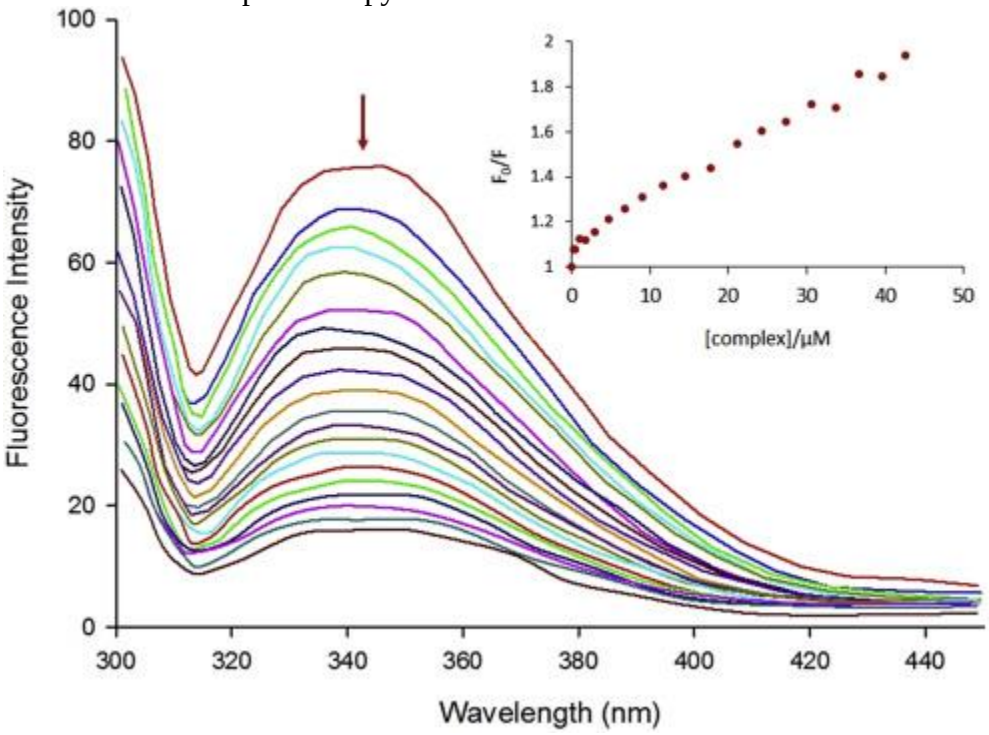

Fig. 7. Fluorescence spectra of HSA (3×10^{-6} M) in the presence of increasing amounts of **(VOL)$_2$O** (3×10^{-5} M), λ_{ex} = 295 nm.

2.3.3. Circular dichroism

Next, in order to study impact of the V(V) complex on the secondary structure of HSA and also to investigate the conformation of protein quantitatively, circular dichroism (CD) spectra of HSA was recorded in the absence and presence of the V(V) complex. The band intensities of HSA decreased in negative ellipticity upon the binding of this complex to HSA, which indicates the decrease of α-helical content and increase of disorder structure and β-sheet contents of HSA (Fig. 8).

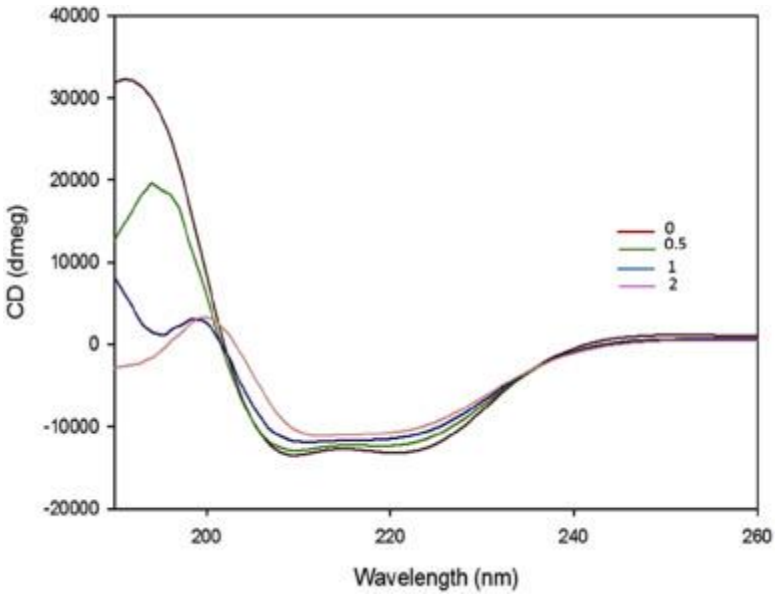

Fig. 8. The CD spectrum of HSA in the absence and presence of the complex, [complex]/[HSA] = 0, 0.5, 1, 2.

The results are expressed in terms of the mean residue ellipticity (MRE) according to Equation (5) [14], [39]:

$$\mathrm{MRE} = \frac{\text{Observed CD (m degree)}}{C_p n l} \times 10 \quad (5)$$

where, C_p is the molar concentration of protein, l is the path length (0.1 cm), n is the number of amino acid residues that is 585 for HSA. The α-helical contents of free and combined HSA can be calculated from MRE values at 208 nm using equation (6):

$$\alpha - \text{helix}\,(\%) = \frac{-MRE_{208} - 4000}{33000 - 4000} \times 100 \quad (6)$$

where, MRE_{208} is the observed mean residue ellipticity value at 208 nm, 4000 is the MRE of the β-sheet and random coil conformation cross at 208, and 33,000 is the MRE value of the pure α-helix at 208 nm.

The α-helical contents of free and combined HSA were calculated from MRE values at 208 nm and are presented in Table 3. As it can be seen, the percentage of α-helix of HSA decreased while those of random coil and β-sheet increased. This observation is due to the formation of HSA-**$(VOL)_2O$** complex.

Table 3. Changes in the secondary structure of HSA upon its interaction with **$(VOL)_2O$** in different concentration (R = [complex]/HSA).

R	**HSA+$(VOL)_2O$**			
	0	**0.5**	**1**	**2**
α-Helix	58.9	54.6	40.70	36.9

R	HSA+(VOL)$_2$O			
	0	**0.5**	**1**	**2**
β-Sheet	20.4	24.0	28.2	29.9
Random coil	19.7	20.4	30.10	32.2

2.3.4. Energy transfer between HSA and V(V) complex

Energy transfer between V(V) complex and HSA can provide valuable information about its HSA binding. The fluorescence quenching of HSA upon its binding to metal complex can be indicative of energy transfer between HSA and metal complex. This energy transfer can be explained by fluorescence resonance energy transfer (FRET) theory. FRET also known as Förster's resonance energy transfer which is an interaction between the excited molecule and its adjacent molecule. Upon this interaction, energy absorbed by donor molecule is transferred to an acceptor [40]. The distance and efficiency of energy transfer (*E*) between tryptophan residue of protein (HSA) and drug (complex) has been calculated, using this theory through the following equation [41]:

$$E = 1 - \frac{F}{F_0} = \frac{R_0^6}{R_0^6 + r^6} \quad (7)$$

where R_0 is the critical distance when the transfer efficiency is 50%; r is the distance between donor and acceptor. R_0 can be calculated by Eq. (8) [41]:

$$R_0{}^6 = 8.79 \times 10^{-25} K^2 N^{-4} J \varphi \quad (8)$$

In the above equation, the term K^2 is the orientation factor of the dipoles; N is the refracted index of medium, J is the overlap integral of the fluorescence spectrum of the donor with absorption spectrum of the acceptor and φ is the fluorescence quantum yield of the donor. The value of J can be calculated by the following expression:

$$J = \frac{\sum F(\lambda)\varepsilon(\lambda)\lambda^4 \Delta\lambda}{\sum F(\lambda)\Delta\lambda} \quad (9)$$

where, F(λ) is the fluorescence intensity of the donor in the absence of the acceptor at wavelength λ and ε is the molar absorption coefficient of the acceptor at λ. In the present case, $K^2 = 2/3$, N = 1.336 and φ = 0.15 for HSA. According to Equations (7), (8), (9) the values of the parameters for the V(V) complex were $J = 2.7 \times 10^{-14}$ cm^3 L mol^{-1}, $R_0 = 3.02$ nm, E = 0.41 and r = 3.22 nm. Fig. S5 represents the overlap of the fluorescence emission spectrum of HSA (3 μM) and the UV–Vis spectrum of the complex (3 μM).

2.3.5. Molecular docking of the V(V) complex with HSA

The V(V) complex was docked to the crystal structure of HSA (Fig. 9). The blind docking on HSA showed that the complex prefers the binding pocket in the cleft of protein with the binding energy about −8.17 kcal mol^{-1}. As it is clear in Fig. 9, there are two hydrogen bonds between V(V) complex and HSA amino acids, with ARG222 and ARG218. In addition, there are two π-cation interactions between the complex and LYS436, LYS195 amino acid residues. The results also indicated that there are hydrophobic contacts between the complex and CYS448, VAL293 and VAL343 amino acid residues. The hydrophilic amino acid residues of HSA, ARG222, ARG218, LYS436, LYS195, ASP451 and TYR452, are also involved in the interaction with the complex.

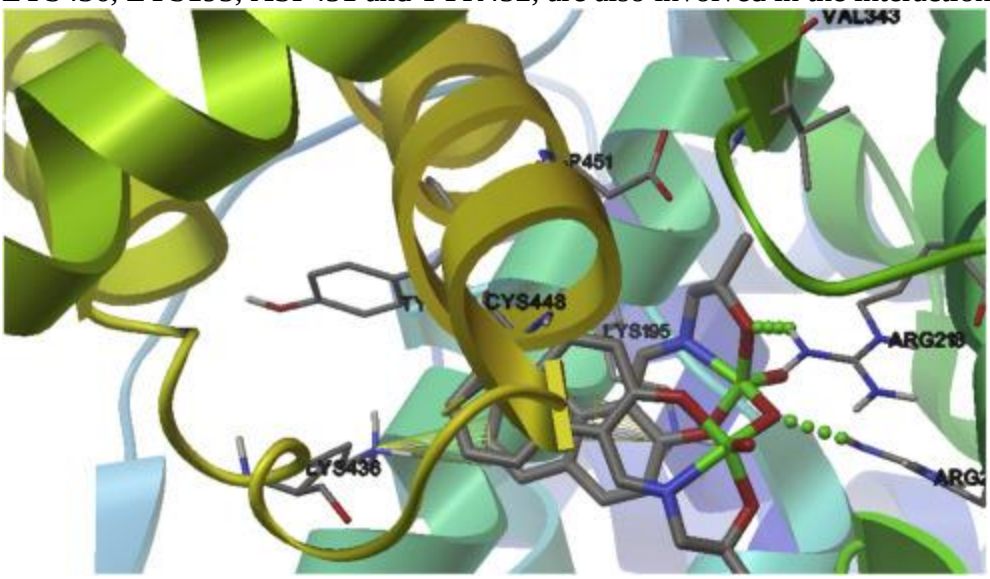

Fig. 9. Docking poses of $(VOL)_2O$ in the active site of HSA, the green dashed line and conical shapes show hydrogen bond and π-cation interactions, respectively. (For interpretation of the references to colour in this figure legend, the reader is referred to the web version of this article.)

2.4. Cell viability assay

MTT assay was used to elucidate the anti-proliferative potential of V(V) complex on two important cancer cell lines including MCF-7 and HeLa and also its adverse effects on normal human fibroblast cells. The results clearly showed the significant anticancer activity of the complex (Fig. 10). The maximum mortality of 74.14% MCF-7 cancer cells and 89.3% HeLa cancer cells obtained after 48 h exposure to 100 μM of the complex. IC50 values of 14 and 36 μM obtained for MCF-7 and HeLa cancer cells, respectively. These results clearly indicate the dose- and cell line-dependent anticancer activity of the complex. Interestingly, the toxic effects of the complex on the normal fibroblast cells were significantly less than cancer cells, as the maximum cell mortality of 12.3% obtained after 48 h incubation of fibroblast cells with 100 μM of the complex. The results indicated the higher anticancer activity of the synthesized complex than previously reported vanadium complexes [42], [43], [44]. Moreover, the complex showed low toxicity on normal human fibroblast cells that is critical for the development of antitumor agents. To the best of our knowledge, it is the first report about the synthesis of anticancer V(V) complex without cytotoxicity on non-cancerous cells.

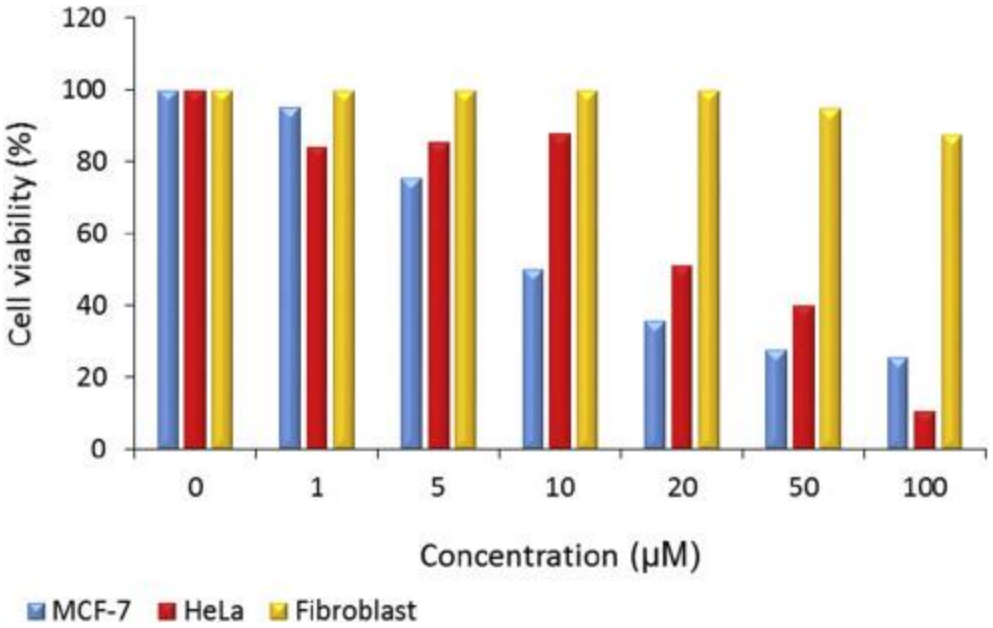

Fig. 10. The viability percentage of MCF-7, HeLa cancer cells and normal fibroblast cells after treatment with different concentrations of V(V) complex for 48 h.

Optical microscopic studies were also used to further evaluate the cytotoxicity of the complex. The results showed the significant morphological changes of the cancer cells following exposure to V(V) complex. The changes in cell morphology were different based on the concentration and cell line which confirm the results of MTT assay. These morphological changes predominantly include cell shrinkage and rounding following with the suppression of cell growth and finally the cell clumping and death (Fig. 11).

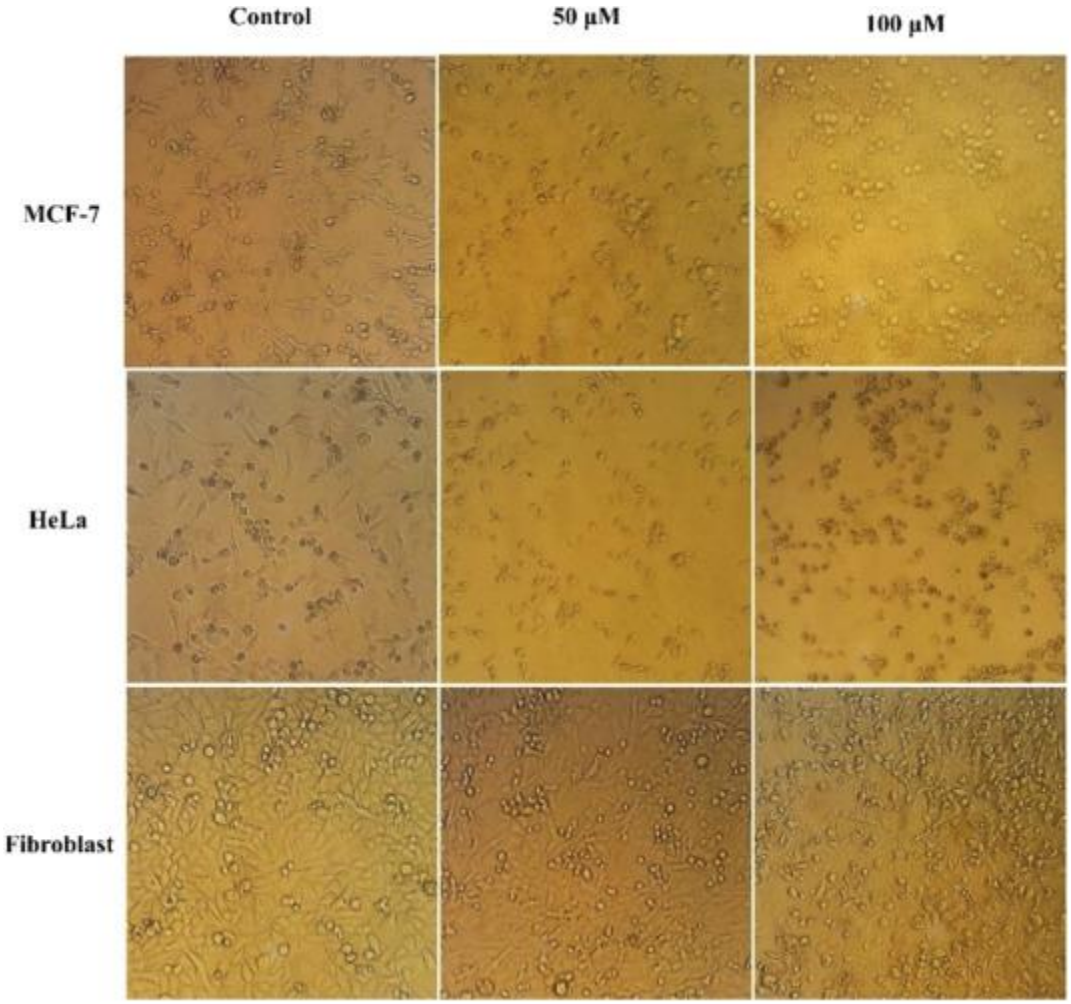

Fig. 11. Morphological changes of normal (fibroblast) and cancer (HeLa and MCF-7) cells after incubation with V(V) complex for 48 h.

3. Conclusion

In summary, we have synthesized a novel dinuclear vanadium complex using a racemic Schiff base ligand. Although there are possibility to form four isomers upon complexation, the isolated complex was as homochiral isomer solely, $(VO(S,S\text{-L}))_2O$ and $(VO(R,R\text{-L}))_2O$, due to ligand self-recognition. The formation of the homochiral isomer and lack of the heterochiral one was confirmed by single-crystal X-ray analysis and NMR technique. DNA- and HSA-binding of the complex were investigated and its binding constants were calculated as 1.9×10^5 and 8.0×10^4 M^{-1}, respectively. In addition, the anticancer activity of this dinuclear metal complex, homochiral isomer, was evaluated. Interestingly, in vitro cytotoxicity assay revealed the potent anticancer activity of this complex on two cancer cell lines (MCF-7 and HeLa), with considerably low toxicity on normal human fibroblast cells. The overall results firmly indicate high potential of this complex for development of therapeutic agents for cancer therapy. Further investigation regarding to the investigation of the mechanism of anticancer activity of V(V) complex and also

development of targeted delivery systems for its efficient and specific delivery to the related tumors could be suggested toward attaining this goal.

4. Experimental

4.1. Chemicals and instrumentation

All required materials were purchased from Sigma-Aldrich except 2-Hydroxy-1-naphtaldehhyde and (*R/S*)-1-aminopropan-2-ol that were obtained from Merck Co. The FT-IR spectrum was recorded on a JASCO, FT/IR-6300 spectrometer (4000–400 cm^{-1}) in KBr pellets. The elemental analysis was performed on Leco, CHNS-932 and Perkin-Elmer 7300 DV elemental analyzers. The UV–Vis spectra were recorded on a JASCO V-670 spectrophotometer. Fluorescence measurements were carried out on Shimadzu RF-5000 spectrofluorometer at room temperature. The circular dichroism (CD) spectra were recorded using Aviv spectropolarimeter model 215 (Proterion Corp., USA) at 25 °C.

4.2. Preparation of V(V) complex

Methanolic solution (10 ml) of 2-hydroxy-1-naphtaldehyde (5 mmol) was added dropwise to a methanolic solution (10 ml) of (*R/S*)-1-aminopropan-2-ol (5 mmol). After continuously stirred for 4 h in ambient temperature, solution of triethylamine (7 mmol) in absolute methanol (5 ml) was added to the solution. The mixture stirred for 30 min, and then a solution of $VO(acac)_2$ (5 mmol) in absolute methanol (20 ml) was added. The solution was stirred for 6 h to proceed completely in ambient temperature. The resulting powder was isolated by filtration and washed by dry methanol several times. The utilize a racemic ligand leads to synthesis complex in four different isomers, (VO-(*R,R/S,S)*-L)$_2$O and (VO-(*R,S)*-L)$_2$O. However, the slow evaporation solution of the vanadium complex in tetrahydrofuran (THF) gave yellow crystals suitable for crystallography that shows only the structure of (VO-(*R,R/S,S)*-L)$_2$O homochiral complex. The typical yield was 81%. Anal. calc. for $C_{30}H_{30}V_2N_2O_7$: C: 56.97, H: 4.78, N: 4.43. Found: C: 60.01, H: 4.98, N: 5.12. Selected IR data (KBr, cm^{-1}): 1621 (νC = N), 1541 (νC—N), 1339 (νC—O). ^{1}H NMR and ^{13}C NMR are presented in Figs. S1 and S2, respectively.

4.3. Single crystal diffraction studies

X-ray data for **(VOL)$_2$O** was collected on a STOE IPDS-II diffractometer with graphite monochromated Mo Karadiation. A yellow crystal was chosen using a polarizing microscope and was mounted on a glass fiber which was used for data collection. Data were collected at 298(2) K in a series ω scans in 1° oscillations and integrated using the StöeX-AREA [45] software package. A numerical absorption correction was applied using the X-RED [46] and X-SHAPE [47] software for V(V) complex. The data were corrected for Lorentz and Polarizing effects. The structures were solved by direct methods using SIR2004. The non-hydrogen atoms were refined anisotropically by the full-matrix least-squares method on F^2 using SHELXL [48]. All hydrogen atoms were added at ideal positions and constrained to ride on their parent atoms. Crystallographic data are listed in Table 1. Selected bond distances and angles are summarized in Table 2.

4.4. DNA binding studies

The stock solution of FS-DNA was prepared in 50 mM Tris buffer at pH 7.5 using double-distilled deionized water and stored at 4 °C. The FS-DNA concentration per nucleotide was determined by the absorption intensity at 260 nm after adequate dilution with the buffer and using the reported molar absorptivity of 6600 M^{-1} cm^{-1}. Purity of FS-DNA solution was confirmed by ratio of UV absorbance at 260 and 280 nm (A_{260}/A_{280} = 1.9), indicating that FS-DNA is free from protein impurity [49]. The solution of the complex was first prepared in DMSO, and then diluted with corresponding buffer to required concentration for all experiments. The volume of DMSO never exceeded 0.3% (v/v), so its effect is negligible. The UV–Vis spectral features of the complex did not change on keeping its buffered or DMSO solution for 24 h and no precipitation or turbidity was observed even after long storage at room temperature, indicating the stability of the complex in different media. However, all the solutions were used freshly after preparation.

The binding character of V(V) complex toward FS-DNA has been investigated by UV–Vis spectroscopy. Spectrophotometric titration experiments were performed by addition of various amounts of DNA (2×10^{-4} M) to V(V) complex (2×10^{-5} M). At each titration step, the mixture solutions were allowed to incubate for 2 min before recording the related spectra. In addition, the equal amounts of DNA solution was added to the blank solution to eliminate its absorbance.

The DNA-binding constant of the complex was also determined by analyzing the fluorescence data obtained from titration of DNA-EthBr with the complex at room temperature. To this aim, a mixture solution of FS-DNA and EthBr at molar ratio of 10: 1 was stirred for 1 h at 4 °C. Then, various amounts of the complex (2.5×10^{-4} M) were added to this mixture. The fluorescence spectra upon the titration were recorded in the range of 550–700 nm with exciting wavelength at 520 nm. The fluorescence quenching experiment was carried out using quartz cuvette with 1 cm optical path length. In each measurement, the complex–DNA solutions were allowed to incubate for 2 min before recording.

4.5. HSA binding studies

A stock solution of HSA was prepared by dissolving the desired amount of HSA in 50 mM phosphate buffer (pH = 7). The HSA stock solution was stored at 4 °C in the dark and used within 2 h. Its concentration was determined by UV–Vis spectrophotometry using the molar absorption coefficient 35,700 M^{-1} cm^{-1} at 278 nm [14]. Absorption titration experiment, an operational and very easy method, was carried out to investigate the HSA-binding of complex at room temperature. The UV–Vis absorption spectra of the HSA solution (7×10^{-6} M) in the absence and presence of various amounts of V(V) complex ($0–35 \times 10^{-6}$ M) were recorded after 2 min incubation.

Fluorescence quenching experiment was also performed to study HSA-binding of the complex. In this experiment 2 ml of HSA solution (3×10^{-6} M) was placed into the cell while various amounts of the complex ($0–15 \times 10^{-6}$ M) were added to the cell at room temperature. The fluorescence intensity was measured with excitation wavelength at 295 nm and emission wavelength rang of 300–450 nm. In each measurement the mixture was allowed to incubate for 2 min after addition of the complexes. The absorptions of HSA at the excitation and emission wavelengths is approximately zero in all concentrations. Hence, a reduction in the emission intensity is independent of the inner filter effect.

Furthermore, the CD spectrum of HSA solution was recorded before and after addition of the complex with molar ratio 0, 0.5, 1 and 2.

4.6. Molecular docking simulation

In this work, docking study was carried out to indicate the DNA and HSA-binding site for the complex. The 3D structures of (*R*,*R*)-**(VOL)$_2$O** complex was generated using the CIF files of its X-ray crystal structures. The CIF files were converted to the PDB format by using the Mercury software (http://www.ccdc.cam.ac.uk/). The known crystal structure of DNA (PDB ID: 423D) with sequence d(ACCGACGTCGGT)2 and HSA (PDB ID: 1AO6) were taken from the Brookhaven Protein Data Bank (http://www.rcsb.org/pdb) at resolution of 1.60 and 2.5 Å, respectively. Water molecules of the .pdb files were removed, missing hydrogen atoms and Gasteiger charges were added. Flexible-ligand docking was performed by AutoDock 4.2 molecular-docking program using the implemented empirical free energy function and the Lamarckian Genetic Algorithm [50]. The Gasteiger charges were added to prepare the macromolecule input files for docking and the Auto Grid was used to calculate Grids. A blind docking with 126 lattice points along X, Y, and Z axes was performed to find the active site of ligands to the biomacromolecules. After determination of the active site, the dimensions of the grid map were selected 60 points with a grid point spacing of 0.375 Å, to allow the ligand to rotate freely. 200 docking runs with 25,000,000 energy evaluations for each run were performed.

4.7. In vitro anticancer activity evaluation

The anticancer activity of the complex was investigated on human breast (MCF-7) and cervical (HeLa) cancer cell lines using MTT assay as described previously [51], [52]. The cytotoxicity of the complex was also studied on the normal human fibroblast cells. To this aim, the cells were first cultured at 37 °C with 5% CO_2 for two weeks. The cells were then seeded on 96-well plates at a density of 10^4 cells per mL and cultured overnight at the same conditions. Following the incubation of the cells with various concentrations (0, 1, 5, 10, 20, 50 and 100 μM) of the complex for 48 h, the medium was discarded and 100 μL MTT (0.5 mg mL^{-1} in media) was added into each well and incubated again at 37 °C for 4 h. The resulting formazan crystals were then dissolved in 100 μL DMSO and the absorbance was measured at 570 nm. The cultured cells in the same condition but without treatment were served as control. Three independent experiments were conducted for each toxicity endpoint. The cell viability was determined as ratio of absorbance values from each treatment and the control. The changes in morphology of the cells after exposure to the corresponding concentrations of the complex were also investigated by using the optical microscope.

Appendix A. Supplementary data

Supplementary data related to this article can be found at http://
dx.doi.org/10.1016/j.ejmech.2017.04.053.

References

[1] W. Liu, J. Ye, M. Jin, Enantioselective phytoeffects of chiral pesticides, J. Agric. Food. Chem. 57 (2009) 2087e2095.
[2] C.-H. Ng, W.-S. Wang, K.-V. Chong, Y.-F. Win, K.-E. Neo, H.-B. Lee, S.-L. San, R.N.Z.R.A. Rahman, W.K. Leong, Ternary copper (II)-polypyridyl enantiomers: aldol-type condensation, characterization, DNA-binding recognition, BSAbinding and anticancer property, Dalton Trans. 42 (2013) 10233e10243.
[3] H. Amouri, M. Gruselle, Chirality in Transition Metal Chemistry: Molecules,

Supramolecular Assemblies and Materials, John Wiley & Sons, 2008.
[4] S.G. Telfer, T. Sato, R. Kuroda, J. Lefebvre, D.B. Leznoff, Dinuclear complexes of chiral tetradentate pyridylimine ligands: diastereoselectivity, positive cooperativity, anion selectivity, ligand self-sorting based on chirality, and magnetism, Inorg. Chem. 43 (2004) 421e429.
[5] J.M. Rowland, M.M. Olmstead, P.K. Mascharak, Chiral monomeric and homochiral dimeric copper (II) complexes of a new chiral ligand, N-(1, 2-Bis (2-pyridyl) ethyl) pyridine-2-carboxamide: an example of molecular self-recognition, Inorg. Chem. 41 (2002) 1545e1549.
[6] N.J. Wheate, J.G. Collins, Multi-nuclear platinum complexes as anti-cancer drugs, Coord. Chem. Rev. 241 (2003) 133e145.
[7] N. Farrell, Metal complexes as drugs and chemotherapeutic agents, Compr. Coord. Chem. 9 (2003) 809e840.
[8] N. Farrell, Y. Qu, L. Feng, B. Van Houten, A comparison of chemical reactivity, cytotoxicity, interstrand crosslinking and DNA sequence specificity of bis (platinum) complexes containing monodentate or bidentate coordination spheres with their monomeric analogs, Biochemistry 29 (1990) 9522e9531.
[9] J.C. Pessoa, S. Etcheverry, D. Gambino, Vanadium compounds in medicine, Coord. Chem. Rev. 301 (2015) 24e48.
[10] M.-j. Xie, X.-D. Yang, W.-p. Liu, S.-p. Yan, Z.-h. Meng, Insulin-enhancing activity of a dinuclear vanadium complex: 5-chloro-salicylaldhyde ethylenediamine oxovanadium (V) and its permeability and cytotoxicity, J. Inorg. Biochem. 104 (2010) 851e857.
[11] A.E. do Amaral, C.L.O. Petkowicz, A.L.R. Merc^e, M. Iacomini, G.R. Martinez, M.E.M. Rocha, S.M.S.C. Cadena, G.R. Noleto, Leishmanicidal activity of polysaccharides and their oxovanadium (IV/V) complexes, ýEur. J. Med. Chem. 90 (2015) 732e741.
[12] H.K. Noor-ul, N. Pandya, N.C. Maity, M. Kumar, R.M. Patel, R.I. Kureshy, S.H. Abdi, S. Mishra, S. Das, H.C. Bajaj, Influence of chirality of V (V) Schiff base complexes on DNA, BSA binding and cleavage activity, ýEur. J. Med. Chem. 46 (2011) 5074e5085.
[13] O.J. D'Cruz, F.M. Uckun, Metvan: a novel oxovanadium (IV) complex with broad spectrum anticancer activity, Expert Opin. Investig. Drugs 11 (2002) 1829e1836.
[14] Z. Kazemi, H. Amiri Rudbari, M. Sahihi, V. Mirkhani, M. Moghadam, S. Tangestaninejad, I. Mohammadpoor-Baltork, G. Azimi, S. Gharaghani, A.A. Kajani, Synthesis, characterization and separation of chiral and achiral diastereomers of Schiff base Pd (II) complex: a comparative study of their DNA-and HSA-binding, J. Photochem. Photobiol. B 163 (2016) 246e260.
[15] D.J. Adams, L.R. Morgan, Tumor physiology and charge dynamics of anticancer drugs: implications for camptothecin-based drug development, Curr. Med. Chem. 18 (2011) 1367e1372.
[16] S. Sanli, Y. Altun, G. Guven, Solvent effects on p K a values of some anticancer agents in acetonitrileewater binary mixtures, J. Chem. Eng. Data 59 (2014) 4015e4020.

[17] C. Kantar, H. Akal, B. Kaya, F. Islamo_glu, M. Türk, S. S¸ as¸maz, Novel phthalocyanines

containing resorcinol azo dyes; synthesis, determination of pKa values, antioxidant, antibacterial and anticancer activity, J. Organomet. Chem. 783 (2015) 28e39.
[18] C. Kantar, V. Mavi, N. Baltas¸ , F. _Islamo_glu, S. S¸ as¸maz, Novel zinc (II) phthalocyanines bearing azo-containing schiff base: determination of pKa values, absorption, emission, enzyme inhibition and photochemical properties, J. Mol. Struct. 1122 (2016) 88e99.
[19] Y.H. Xing, K. Aoki, F.Y. Bai, Synthesis and crystal structure of a vanadium (V) complex with 1, 10-phenanthroline ligand, VO2 (acac)(1, 10-phen), as an insulin mimic, Synth. React. Inorg. Met.-Org. Chem. 33 (2003) 1801e1809.
[20] C. Datta, D. Das, P. Mondal, B. Chakraborty, M. Sengupta, C.R. Bhattacharjee, Novel water soluble neutral vanadium (IV)eantibiotic complex: antioxidant, immunomodulatory and molecular docking studies, ýEur. J. Med. Chem. 97 (2015) 214e224.
[21] Z. Kazemi, H. Amiri Rudbari, V. Mirkhani, M. Sahihi, M. Moghadam, S. Tangestaninejad, I. Mohammadpoor-Baltork, Synthesis, characterization, crystal structure, DNA-and HSA-binding studies of a dinuclear Schiff base Zn (II) complex derived from 2-hydroxynaphtaldehyde and 2-picolylamine, J. Mol. Struct. 1096 (2015) 110e120.
[22] C. Cordelle, D. Agustin, J.-C. Daran, R. Poli, Oxo-bridged bis oxo-vanadium (V) complexes with tridentate Schiff base ligands (VOL) 2 O (L¼ SAE, SAMP, SAP): synthesis, structure and epoxidation catalysis under solvent-free conditions, Inorg. Chim. Acta 364 (2010) 144e149.
[23] S.-J. Li, K. Li, X.-Y. Qiu, X.-J. Yao, Two new isomeric di-m-oxo bis [oxovanadium (V)] complexes containing schiff base ligands, J. Chem. Crystallogr. 42 (2012) 879e883.
[24] N. Noshiranzadeh, M. Emami, R. Bikas, J. Sanchiz, M. Otre¸ba, P. Aleshkevych, T. Lis, Synthesis, characterization and magnetic properties of a dinuclear oxidovanadium (IV) complex: magneto-structural DFT studies on the effects of out-of-plane-OCH 3 angle, Polyhedron (2016) 194e202.
[25] A. Sarkar, S. Pal, Divanadium (V) complexes with 4-R-benzoic acid (1-methyl-3-oxo-butylidene)-hydrazides: syntheses, structures and properties, Inorg. Chim. Acta 362 (2009) 3807e3812.
[26] A.-C. Schmidt, M. Hermsen, F. Rominger, R. Dehn, J.H. Teles, A. Sch€afer, O. Trapp, T. Schaub, Synthesis of mono-and dinuclear vanadium complexes and their reactivity toward dehydroperoxidation of alkyl hydroperoxides, Inorg. Chem. (2017) 1319e1332.
[27] S.S. Bhat, A.A. Kumbhar, H. Heptullah, A.A. Khan, V.V. Gobre, S.P. Gejji, V.G. Puranik, Synthesis, electronic structure, DNA and protein binding, DNA cleavage, and anticancer activity of fluorophore-labeled copper (II) complexes, Inorg. Chem. 50 (2010) 545e558.
[28] X. Wang, M. Yan, Q. Wang, H. Wang, Z. Wang, J. Zhao, J. Li, Z. Zhang, In vitro DNA-binding, anti-oxidant and anticancer activity of indole-2-carboxylic acid dinuclear copper (II) complexes, Molecules 22 (2017) 171e184.
[29] K. Hu, F. Li, Z. Zhang, F. Liang, Synthesis of two potential anticancer copper (ii) complex drugs: their crystal structure, human serum albumin/DNA binding

and anticancer mechanism, New J. Chem. 41 (2017) 2062e2072.
[30] S.U. Dighe, S. Khan, I. Soni, P. Jain, S. Shukla, R. Yadav, P. Sen, S.M. Meeran, S. Batra, Synthesis of b-carboline-based N-Heterocyclic carbenes and their antiproliferative and antimetastatic activities against human breast cancer cells, J. Med. Chem. 58 (2015) 3485e3499.
[31] B. Demoro, R.F. de Almeida, F. Marques, C.P. Matos, L. Otero, J.C. Pessoa, I. Santos, A. Rodríguez, V. Moreno, J. Lorenzo, Screening organometallic binuclear thiosemicarbazone ruthenium complexes as potential anti-tumour agents: cytotoxic activity and human serum albumin binding mechanism, Dalton Trans. 42 (2013) 7131e7146.
[32] F. Li, M. Feterl, J.M. Warner, A.I. Day, F.R. Keene, J.G. Collins, Protein binding by dinuclear polypyridyl ruthenium (II) complexes and the effect of cucurbit [10] uril encapsulation, Dalton Trans. 42 (2013) 8868e8877.
[33] Z. Kazemi, H.A. Rudbari, M. Sahihi, V. Mirkhani, M. Moghadam, S. Tangestaninejad, I. Mohammadpoor-Baltork, S. Gharaghani, Synthesis, characterization and biological application of four novel metal-Schiff base complexes derived from allylamine and their interactions with human serum albumin: experimental, molecular docking and ONIOM computational study, J. Photochem. Photobiol. B 162 (2016) 448e462.
[34] F.J. Fard, Z.M. Khoshkhoo, H. Mirtabatabaei, M. Housaindokht, R. Jalal, H.E. Hosseini, M. Bozorgmehr, A. Esmaeili, M.J. Khoshkholgh, Synthesis, characterization and interaction of N, N0-dipyridoxyl (1, 4-butanediamine) Co (III) salen complex with DNA and HSA, Spectrochim. Acta A 97 (2012) 74e82.
[35] O.K. Abou-Zied, Revealing the ionization ability of binding site I of human serum albumin using 2-(20-hydroxyphenyl) benzoxazole as a pH sensitive probe, Phys. Chem. Chem. Phys. 14 (2012) 2832e2839.
[36] E.M. Mrkali_c, R.M. Jeli_c, O.R. Klisuri_c, Z.D. Matovi_c, Synthesis of novel palladium (II) complexes with oxalic acid diamide derivatives and their interaction with nucleosides and proteins. Structural, solution, and computational study, Dalton Trans. 43 (2014) 15126e15137.
[37] K. Laskar, P. Alam, R.H. Khan, A. Rauf, Synthesis, characterization and interaction studies of 1, 3, 4-oxadiazole derivatives of fatty acid with human serum albumin (HSA): a combined multi-spectroscopic and molecular docking study, ýEur. J. Med. Chem. 122 (2016) 72e78.
[38] S.U. Dighe, S. Khan, I. Soni, P. Jain, S. Shukla, R. Yadav, P. Sen, S.M. Meeran, S. Batra, Synthesis of b-carboline-based N-heterocyclic carbenes and their antiproliferative and anti-metastatic activities against human breast cancer cells, J. Med. Chem. 58 (8) (2015) 3485e3499.
[39] X. Li, S. Wang, Study on the interaction of (þ)-catechin with human serum albumin using isothermal titration calorimetry and spectroscopic techniques, New J. Chem. 39 (2015) 386e395.
[40] N. Fani, A. Bordbar, Y. Ghayeb, A combined spectroscopic, docking and molecular dynamics simulation approach to probing binding of a Schiff base complex to human serum albumin, Spectrochim. Acta Mol. Biomol. Spectrosc. 103 (2013) 11e17.
[41] F. Deng, Y. Liu, Study of the interaction between tosufloxacin tosylate and

bovine serum albumin by multi-spectroscopic methods, J. Lumin. 132 (2012) 443e448.
[42] I. Correia, S. Roy, C.P. Matos, S. Borovic, N. Butenko, I. Cavaco, F. Marques, J. Lorenzo, A. Rodríguez, V. Moreno, Vanadium (IV) and copper (II) complexes of salicylaldimines and aromatic heterocycles: cytotoxicity, DNA binding and DNA cleavage properties, J. Inorg. Biochem. 147 (2015) 134e146.
[43] B. Balaji, B. Balakrishnan, S. Perumalla, A.A. Karande, A.R. Chakravarty, Photocytotoxic oxovanadium (IV) complexes of ferrocenyl-terpyridine and acetylacetonate derivatives, ýEur. J. Med. Chem. 92 (2015) 332e341.
[44] M.R. Maurya, A.A. Khan, A. Azam, A. Kumar, S. Ranjan, N. Mondal, J.C. Pessoa, Dinuclear oxidovanadium (IV) and dioxidovanadium (V) complexes of 5, 50-methylenebis (dibasic tridentate) ligands: synthesis, spectral characterisation, reactivity, and catalytic and antiamoebic activities, Eur. J. Inorg. Chem. 2009 (2009) 5377e5390.
[45] S. Cie, Program for the Acquisition and Analysis of Data XeAREA, version1. 30, Stoe & Cie GmbH, Darmatadt, Germany, 2005.
[46] S.C. GmbH (Ed.), X-RED, Program for Data Reduction and Absorption Correction, 2005. Darmatadt, Germanny.
[47] C. Stoe, X-SHAPE, Version 2.05, Program for Crystal Optimization for Numerical Absorption Correction, Stoe & Cie GmbH, Darmatadt, Germany, 2004.
[48] G.M. Sheldrick, A short history of SHELX, Acta Crystallogr. Sect. A Found. Crystallogr. 64 (2008) 112e122.
[49] Z. Asadi, N. Nasrollahi, H. Karbalaei-Heidari, V. Eigner, M. Dusek, N. Mobaraki, R. Pournejati, Investigation of the complex structure, comparative DNAbinding and DNA cleavage of two water-soluble mono-nuclear lanthanum (III) complexes and cytotoxic activity of chitosan-coated magnetic nanoparticles as drug delivery for the complexes, Spectrochim. Acta A 178 (2017) 125e135.
[50] G.M. Morris, D.S. Goodsell, R.S. Halliday, R. Huey, W.E. Hart, R.K. Belew, A.J. Olson, Automated docking using a Lamarckian genetic algorithm and an empirical binding free energy function, J. Comput. Chem. 19 (1998) 1639e1662.
[51] J.D. Chellaian, J. Johnson, Spectral characterization, electrochemical and anticancer studies on some metal (II) complexes containing tridentate quinoxaline Schiff base, Spectrochim. Acta Mol. Biomol. Spectrosc. 127 (2014) 396e404.
[52] A.A. Kajani, A.-K. Bordbar, S.H.Z. Esfahani, A. Razmjou, Gold nanoparticles as potent anticancer agent: green synthesis, characterization, and in vitro study, RSC Adv. 6 (2016) 63973e63983.